Chapter 4

Results and Discussion

4.1 Introduction

In this chapter, the low-frequency range mould vibration of the die-cast A308 alloy is discussed as a technique for creating more nucleation sites during melt solidification through fragmentation of dendrites and Si particles. To determine the performance of the as-cast and vibrated cast samples, the physical, metallurgical, and mechanical properties of the samples were analyzed. Therefore, the chapter is divided into four sections (a) Physical properties, (b) Metallurgical properties, (c) Mechanical properties, and (d) Fractography. The chapter concludes with a summary of the results of the physical, metallurgical, and mechanical tests.

4.2 Effects of low-frequency range horizontal mould vibration on the physical, metallurgical, and mechanical properties of die-cast A308 alloy

Today's casting industries strive to produce high-quality cast components in an efficient, cost-effective, eco-friendly, and sustainable way. To achieve this, an indigenously developed, well, controlled digital vibratory setup, this study examines the effect of high amplitude vibration on the density, silicon morphology, and mechanical properties of A308 alloy. The metallurgical alterations were evaluated by optical microscopy, x-ray diffraction analysis, scanning electron microscopy, and energy dispersive spectroscopy. The size of α-Al grains, SDAS, length, width, and aspect ratio of eutectic Si particles decreased by 53%, 63%, 71%, 18%, and 62%, respectively. In comparison, the shape factor and density increased by 39% and 2.5%, respectively. Consequently, yield strength, ultimate tensile strength, % elongation, and microhardness increased by 16%, 25%, 17%, and 42%, respectively, at 2.5 mm amplitude and 10 Hz frequency compared with the conventional casting method. Refinement in eutectic silicon particle size (length, width and aspect ratio) and shape (plate to fibrous), dendrite fragmentation, structural

uniformity, decreased porosities, and subsequent increase in density contributed to this improvement in mechanical properties. The SEM fractographs of tensile test samples showed a transgranular brittle fracture. At 10 Hz frequency, the fracture surfaces exhibit brittle fracture mode with partial ductility.

4.3 Physical properties

4.3.1 Density, porosity and cooling rate

Archimedes' principle was used to calculate the density of cast samples. In this procedure, the weight of the sample was taken in distilled water and air. The density was measured by the equation given below:

$$\rho_{exp} = \frac{W_a}{(W_a - W_L)} \rho_L \quad (1)$$

Where ρ_{exp} and W_a stand for the air's density and weight, whereas W_L and ρ_L stand for the weight and density in distilled water [46], the mass was measured using digital density balance (CAH-503, Contech Instruments Limited, India), having accuracy up to .0001g/cm^3 shown in Fig. 4. The standard deviation of observed experimental densities was calculated using the gauge R&R research.

The theoretical density was measured using the following equation: the mixture rule [86] [22].

$$\rho_{th} = \frac{1}{\sum \frac{W_i}{\rho_i}} \times 100 \quad (2)$$

Where Wi is the weight fraction of ith (Si, Cu, Mn, Fe, Mg, Ti, Zn, V, and Al) elements obtained in chemical composition analysis, as shown in Table 1. ρ_i denotes the theatrical density of ith elements, the theoretically calculated density of the alloy is 2.795 g/cm^3. The density of the stationary cast sample, as determined by the experiment, was 2.724 g/cm^3, the lowest of all the vibratory casting samples. Micro porosities in the interdendritic sections resulted in poor density, as illustrated in the as-cast sample picture

in Fig. 5. (a). Table 3 shows the calculated experimental density of castings under stationary and vibrating conditions. With an increase in the intensity level of vibration, Figs. 5 (b-d) indicates a steady reduction in the size of the porosity defect and, as a result, an increase in the density of the vibratory cast samples. At 10 Hz, the density of the alloy reaches its maximum value of 2.794 g/cm^3. Hence, a 2.5% improvement in the density was observed at a 10 Hz frequency. The porosity size is continuously reducing in Figure 4.1(a-e). As demonstrated in Table 4.1, cooling is 21% quicker due to vibration. Porosity is also reduced by 84% due to improved mass feeding and reduced porosities. Consequently, an increase of 2.5% in the density was obtained at a 10 Hz frequency.

Table 4.1: The density of A308 alloy at (0-10) Hz frequencies

Frequency (Hz)	Weight in the air (g)	Weight in water(g)	Average Density(g/cc)	Standard Deviation
0	15.066	9.555	2.724	0.00265
2	14.059	8.925	2.737	0.00170
4	14.827	9.435	2.748	0.00183
6	15.151	8.977	2.749	0.00337
8	14.547	9.239	2.753	0.00302
10	15.019	9.568	2.794	0.00156

Table 4.2: The cooling rate of casting at (0-10) Hz frequencies

Frequency/ Hz	Pouring Temp.	Freezing Temp.	Freezing Time/ Sec	Cooling Rate °C/ Sec
0	710	520	123	1.54
2	710	520	118	1.61
4	710	520	112	1.69
6	710	520	106	1.79
8	710	520	104	1.82
10	710	520	102	1.86

4.4 Metallurgical observations

4.4.1 Microstructure analysis

The microstructures of Al-Si alloys are made of Al matrix in the hypoeutectic and eutectic ranges, with eutectic Si appearing as a refined fibrous structure as shown in Figure 4.1 [5]. Figure 4.1 displays the optical microscopy images of the alloy under stationary and vibratory conditions. Figure 4.1(a) shows eutectic silicon and SDAS are coarse in size with sizeable interdendritic porosity. Eutectic silicon size, SDAS, and shrinkage pores are reduced gradually by mould vibration, as shown in Figures 4.1(b-f). The optical micrographs at higher magnifications of different samples are shown in Figures 4.2(a-f). A steady microstructure refinement was observed by increasing the vibrational frequencies from 2 Hz to 10 Hz, as illustrated in Figs 4.1 and 4.2(b-f). Microstructural investigation revealed refined eutectic silicon and fractured dendrites at higher frequencies, as illustrated in Figs. 4.1 and 4.2 (d-e). The nucleation rate was increased, eutectic Si growth was limited, and the microstructure was refined with the vibrated mould. It is well known that better grain refinement could be achieved by introducing mould shocks during solidification at some frequency extension. Al-Si alloy is an irregular eutectic alloy and displays complex nucleation and growth behaviour [5].

The microstructure of castings at higher frequencies (8-10 Hz) showed complete dendritic fragmentation, and large dendrites (Typical tree-like structure) disappeared along with refined Al-Si eutectic structure as shown in Figs. 4.2(d-e). Moreover, higher frequency vibration modified the constituent secondary phases of the cast alloy and helped in dispersing them uniformly into the molten alloy, and a homogeneous structure was achieved. It is well known that coarse and acicular eutectic Si causes early failure by acting as first stress raisers [5]. It was observed that the coarse eutectic silicon transformed into small sizes under the mould vibration at a frequency (8-10 Hz), as shown in Fig. 4.2(e-f), which was the desired microstructural characteristic for achieving

better mechanical properties. It was concluded that flake-shaped silicon transformed into fibrous-shaped silicon due to faster cooling [5].

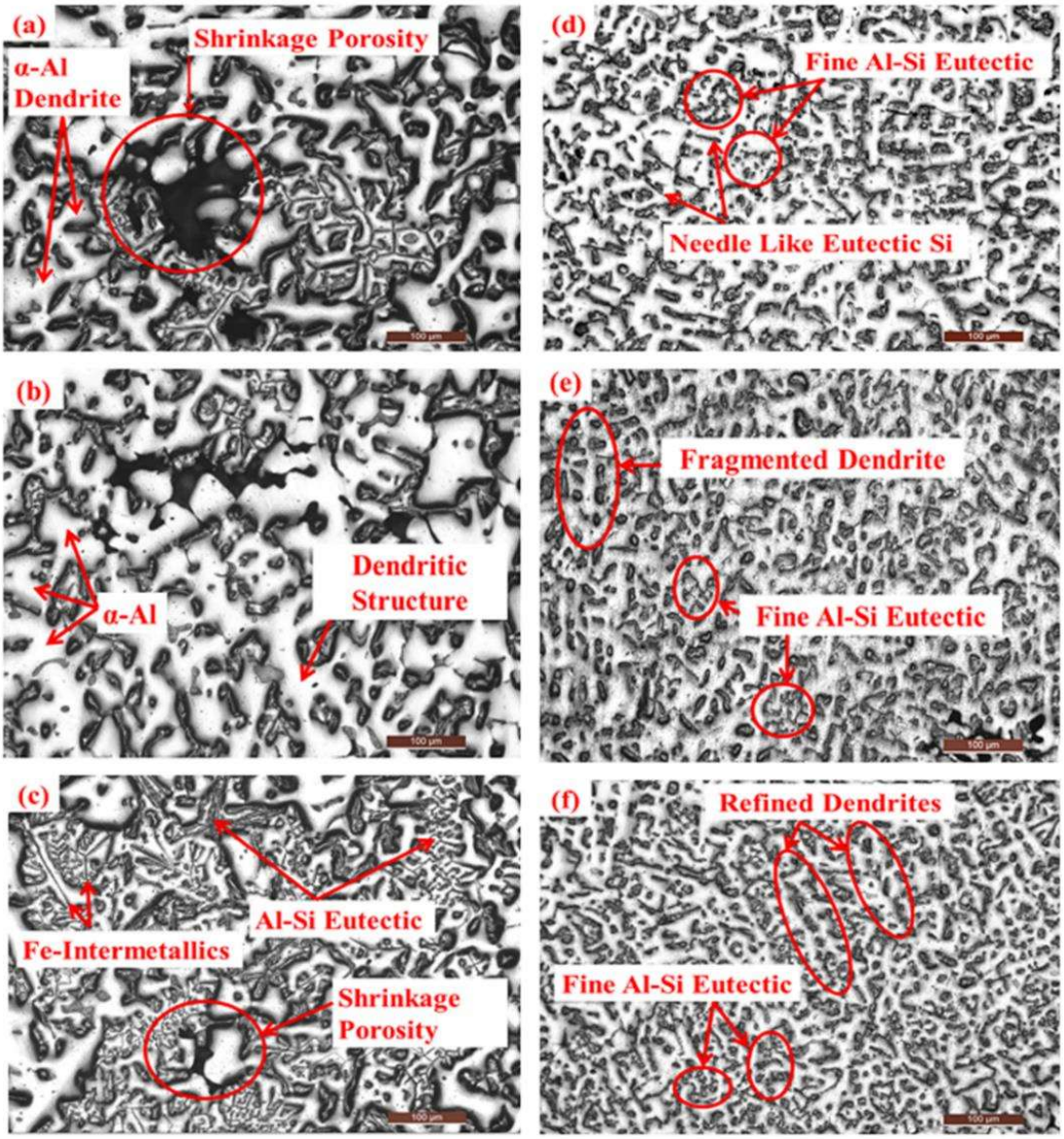

Figure 4.1: Microstructure of A308 alloys (a) Stationary condition, (b) 2 Hz, (c) 4 Hz, (d) 6 Hz, (e) 8 Hz, and (f) 10 Hz.

Simultaneously, alternating tension-pressure forces began dendritic fragmentation on the inner surface of the mould wall, where heterogeneous nucleation began and propagated. The parameters, such as acceleration parameter (f^2*a) or f*a alone, represent the effect of vibration better than frequency (f) or amplitude (a) alone in mechanical vibration

treatment. Due to the acceleration parameter (f^2*a), the relative forces will act better between the molten alloy and mechanical vibration. The higher f^2*a value will ensure greater vibration intensity and more metal convection; as the metal convection intensity increases, α-Al phase morphology changes[14].

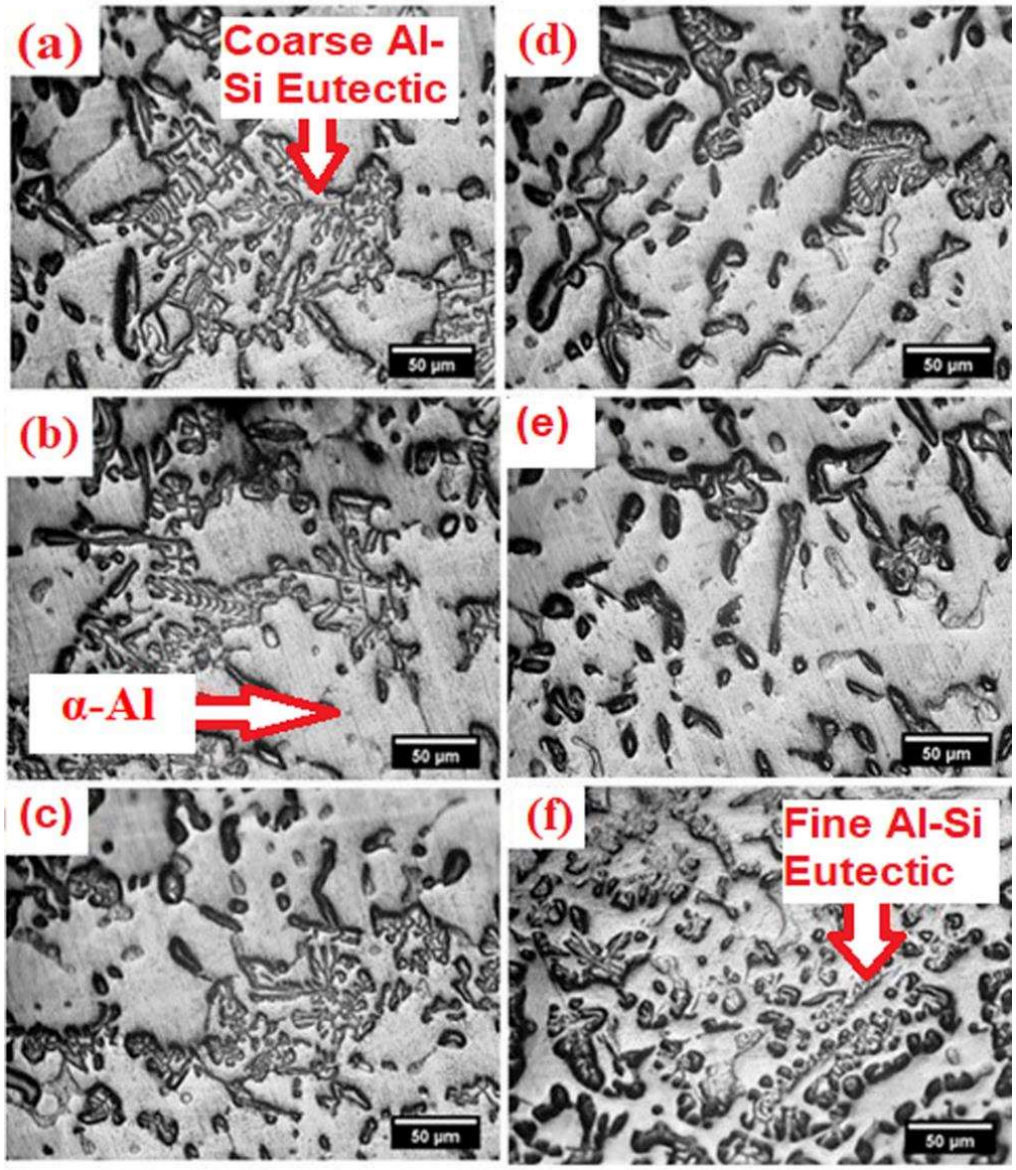

Figure 4.2: Eutectic silicon refinement of A308 alloys (a) stationary condition 0 Hz, (b) 2 Hz, (c) 4 Hz, (d) 6 Hz, (e) 8 Hz, and (f) 10 Hz.

4.4.2 Morphology of the metallurgical features

The changes in the morphology of α-Al size, shape factor, SDAS, length, width, and aspect ratio of Si particles under different frequencies (0-10 Hz) were sum up in Table 4.3 Vibration reduced the size of α-Al, SDAS, length, width, and aspect ratio of Si particles, and improved the shape factor. At 10 Hz, the α-Al, SDAS, length, width, and aspect ratio of Si particles displayed the lowest values, and they are 53%, 63%, 71%, 18%, and 65% lower than stationary cast samples, respectively. On the other hand, the shape factor was highest at 10 Hz, with a 39% improvement compared to stationary casting. As demonstrated in Table 4.3, vibration causes a quicker cooling rate, 17% faster than a stationary casting cooling rate. The heat transfer coefficient is increased by the convection effect caused by vibration [14]. An increase in frequency increases the vibration intensity.

Consequently, the shear force produced is more significant than lower frequencies. Shear force improves the flowability, dendritic fragmentation, and shape factor, shortens the length and widens the width of the eutectic silicon, and reduces the porosity. The aspect ratio of columnar grain is greater than 1, whereas, for equiaxed grains, it is around about 1. The shape factor shows the grain's globularity; if the value of the shape factor is around 1, it shows that the grain is spherical.

Table 4.3: Effect of (0-10) Hz frequency on morphology of metallurgical features

Freq. /Hz	α-Al size/µm	SDAS/µm	Shape factor	Avg. length of eutectic Si /µm	Avg. width of eutectic Si / µm	Aspect ratio of eutectic Si
0	100.25±19.20	75.31±11.6	0.61±0.01	45.96±9.44	7.35 ± 1.62	6.25 ± 1.15
2	76.94±9.35	58.75±8.52	0.65±0.01	40.99±8.07	6.66 ± 1.31	6.15 ± 1.02
4	66.53±8.61	54.29±8.23	0.72±0.02	36.29±7.85	6.53 ± 1.68	5.55 ± 0.93
6	55.79±9.32	45.08±7.72	0.74 0.01	25.82±7.11	6.23 ± 2.01	4.14 ± 0.79
8	52.31 ± 8.98	35.69 ± 7.91	0.80±0.02	17.06±3.61	6.15 ± 1.21	2.77 ± 0.64
10	47.10 ± 9.88	28.21± 6.81	0.85±0.02	14.06±3.21	6.12 ± 1.31	2.35 ± 0.50

4.4.3 Mechanism of dendrite fragmentation

Mould vibration initiated the forced convection in the melt. Simultaneously, an external force acted on the columnar dendrite arms in the direction of melt flow and adequate fragmentations of columnar dendrites in the melt. Induced viscous drag forces may start the separation of dendritic arms. When a viscous drag force separates a dendrite, separated arms come close across neighbouring arms, causing further fragmentation [46] Numerous mechanisms were proposed for dendritic fragmentation, i.e., recrystallisation, shearing, partial remelting in the way of dendritic arms, and showering of dendrites [83]. The solidification time decreases as the cooling rate of the mould vibration increases; hence, more nucleation may occur. The acicular eutectic silicon is converted into a fibrous form after mechanical vibration, as seen in Figures 4.2 (b-f). As seen in Figure 4.2(a), the grain structure of stationary castings was coarser than that of vibratory castings as shown in Figures 4.2(b-f). The vibration effect refines grains and helps to form a non-dendritic structure. Figure 4.2(a-f) shows eutectic silicon refinement at stationary and vibratory conditions. Figure 4.2(a) indicates Al-Si eutectic phases, which are coarser. Still, the coarse eutectic phases were gradually refined with increased vibrational frequency into spherical shapes, as seen in Figure. 4.2(b-f). The maximum refinement in

microstructure was observed at a 10 Hz frequency level due to the more fragmentation of Al-Si eutectic phases, as shown in Fig**.** 4.2(f). It can be observed that dendritic structures transformed into non-dendritic ones after applying vibrations. Mould vibration can break the dendritic stems during solidification and remelt them in the molten alloy. Separated and fragmented dendritic branches generate new nuclei in the molten alloy, and thus refined microstructure is achieved [85].

4.4.4 X-ray Diffraction analysis

An X-ray diffractometer (XRD) and PCPDFWIN-2013 software were used to confirm the secondary phases present in the A308 alloy. The eutectic silicon phases, Al_2Cu, and $Fe_{1.7}SiAl_4$ were established from the analysis, as evident in Figure 4.3. The elements were Al, Si, Cu, and Fe, and intermetallic compounds such as Al_2Cu and $Fe_{1.7}SiAl_4$. Usually, Inter-metallic compounds are brittle and have high melting points. They often offer a trade-off between ceramic and metallic properties. The percentage of Cu content, reactions during solidification, and solute concentration are the major reasons for the precipitation of Al_2Cu intermetallic. Hence the same parameter can be responsible for the formation of Al_2Cu precipitate. Copper reacts with aluminium to generate the Al_2Cu intermetallic phase, which develops during solidification time. Al_2Cu may precipitate in a block-like form immediately from the liquid with a Cu concentration of 53.5 wt. percent, especially in the presence of the β-Fe phase, in the form of eutectic ($Al + Al_2Cu$), or in a mixture of both, depending on the cooling rate and local concentration of segregated Cu atoms. Most commonly, the copper phase forms as small pockets of blocky Al_2Cu nucleating on pre-existing β-Fe platelets. Having an iron content of 0.718% promoted the dispersion of Al_2Cu particles and the formation of the β-Fe phase, which precipitated before the Cu-rich phase, thereby providing nucleation sites for the Cu-rich

phase while simultaneously reducing Al_2Cu phase segregation and, therefore, particle size [87].

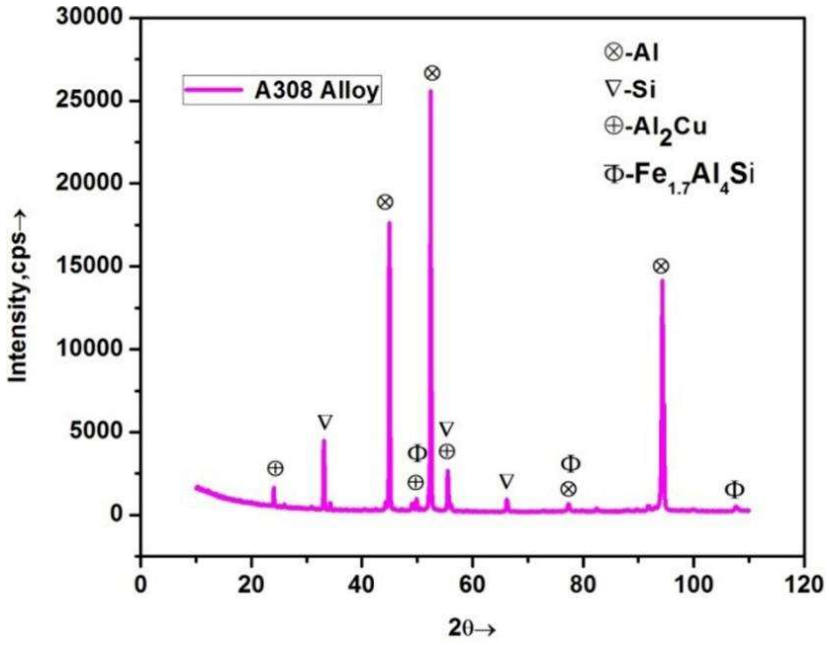

Figure 4.3: X-ray diffraction pattern of A308 alloy

4.4.5 Energy dispersive spectrometer (EDS) analysis

The elemental analysis of the alloy was performed with the EDS technique. The objective of the elemental study was to confirm the presence of the elemental wt.% and EDS spectrum at two selected points are evident in Figure 4.4 (a–b). The elements Si, Cu, Fe, and Al, are shown in Figure 4.4(a), confirming the synthesis of intermetallics such as Fe-Si-Al and Al_2Cu. Bayraktarhe et al. [88] also observed Al_2Cu intermetallic phase in Al-Si alloy with 3% Cu. similarly, the existence of Al, Si, Mn, and Cu, in addition to Fe, was verified in Fig. 4.4(b), indicating the formation of intermetallics such as $Fe_{1.7}SiAl_4$ and Al_2Cu. These findings were entirely consistent with the XRD observations.

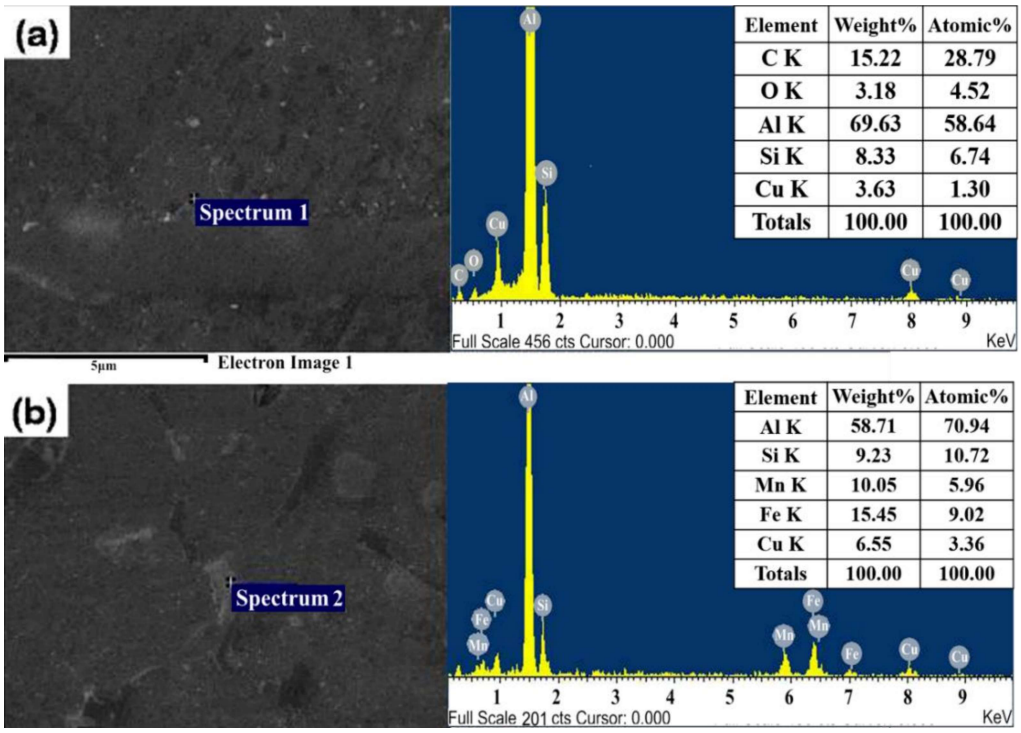

Figure 4.4: EDS spectra of A308 Al Alloy at (a) 8 Hz, and (b) 10 Hz frequencies

4.5 Mechanical properties

4.5.1 Tensile test results

Tensile test results of stationary and vibratory castings are summarised in the Table. 4.4. Mechanical properties, i.e., UTS, YS, %EL, and HV, were improved as the frequency level was increased. The results show that the improvement in YS, UTS, %EL and HV were 16%, 25%, 17%, and 42% at 10 Hz compared to stationary cast samples. It is mainly due to the refinement in the grain size and transition of eutectic silicon from flake to fibre morphology and porosity reduction [5]. The Hall-Petch law also states that improvement in the YS values is inversely proportional to grain size. Therefore, mechanical properties increases as the average grain size reduce [89]. The grain boundaries act as pinning points impeding further dislocation propagation. Since the lattice structure of adjacent grains differs in orientation, it requires more energy for a dislocation to change directions and move into the adjacent grain. The grain boundary is also much more disordered than

inside the grain, which also prevents the dislocations from moving in a continuous slip plane. Impeding this dislocation movement will hinder the onset of plasticity and hence increase the yield strength of the material [8, 11]. The mechanical properties of the alloy may have been improved by refining and spheronization of silicon particles [4].

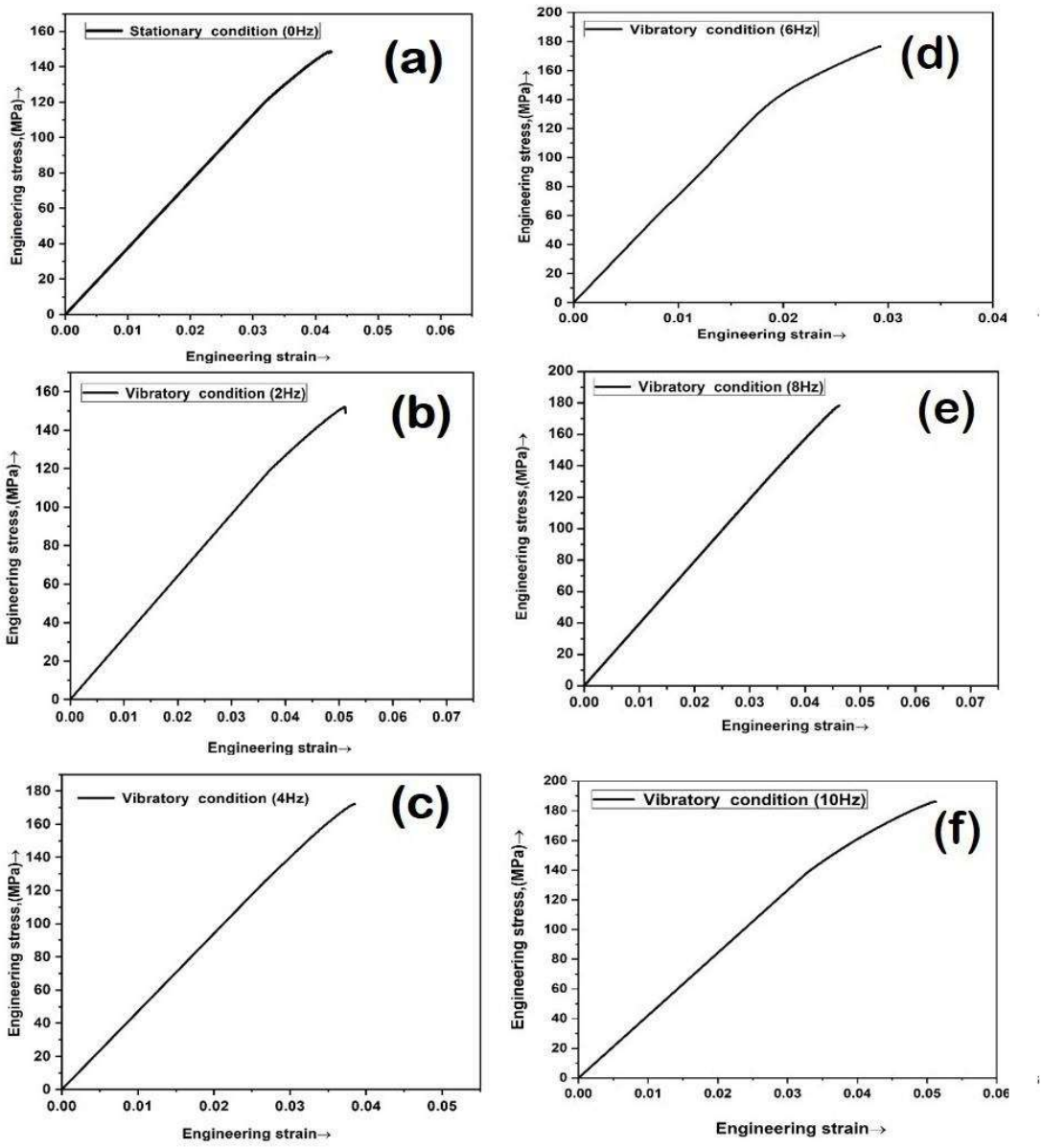

Figure 4.5: Typical engineering stress-strain diagram at (a) stationary condition, (b) 2 Hz, (c) 4 Hz, (d) 6 Hz, (e) 8 Hz and (f) 10 Hz frequencies.

Engineering stress-Engg strain diagrams are shown in Fig. 4.5 for stationary (0 Hz) and vibratory castings (2-10 Hz). The engineering stress-strain diagram under the stationary

casting condition showed a UTS value of around 149 MPa, as evident in Fig. 4.5(a). As the frequency level was increased to 10 Hz, the UTS value increased to 186 MPa, i.e., 25% improved UTS compared to stationary casting. It is mainly due to a 21% faster cooling rate as shown in Table 4.2 and 53% more grain refinement than conventional casting. Table 4.3 shows the precise YS, UTS, %EL, and HV values. Surprisingly, the obtained results reveal two times more YS, UTS, and HV values ascribed to 21% faster cooling rate and 53% more grain refinement, respectively, when compared to the same alloy vibrated at high frequency (0-50 Hz) and low amplitude (31m) [90].

Table 4.4: Effect of (0-10) Hz frequency on mechanical properties of castings

Mechanical vibration parameters						
Power / V	Amplitude / mm	Frequency/ Hz	YS / MPa	UTS / MPa	%El.	HV
0	0	0	119 ± 6.7	149 ± 8.1	3.02 ± 0.3	74 ± 4.7
3.5	2.5	2	120 ± 7.0	152 ± 8.0	3.09 ± 0.3	85 ± 4.5
3.5	2.5	4	125 ± 7.5	172 ± 8.7	3.22 ± 0.4	93 ± 4.8
3.5	2.5	6	137 ± 7.8	176 ± 8.9	3.29 ± 0.3	102 ± 4.6
3.5	2.5	8	138 ± 7.7	178 ± 8.7	3.39 ± 0.4	103 ± 5.0
3.5	2.5	10	140 ± 7.9	186 ± 9.2	3.54 ± 0.5	105 ± 5.2

4.5.2 Hardness measurement

The Vickers hardness values of stationary and vibratory castings were presented in Table 4.4. In stationary casting, the observed value was 74 HV, i.e., the lowest among all the measurements chiefly due to the coarser grain size of eutectic silicon particles and larger dendrite cells. In contrast, at 10 Hz frequency, the value reached 105 HV, which showed a substantial increase, i.e., by 42%. This improvement in the HV value was observed mainly due to a 53% reduction in grain size [89].

4.5.3 Mechanism for hardness improvement

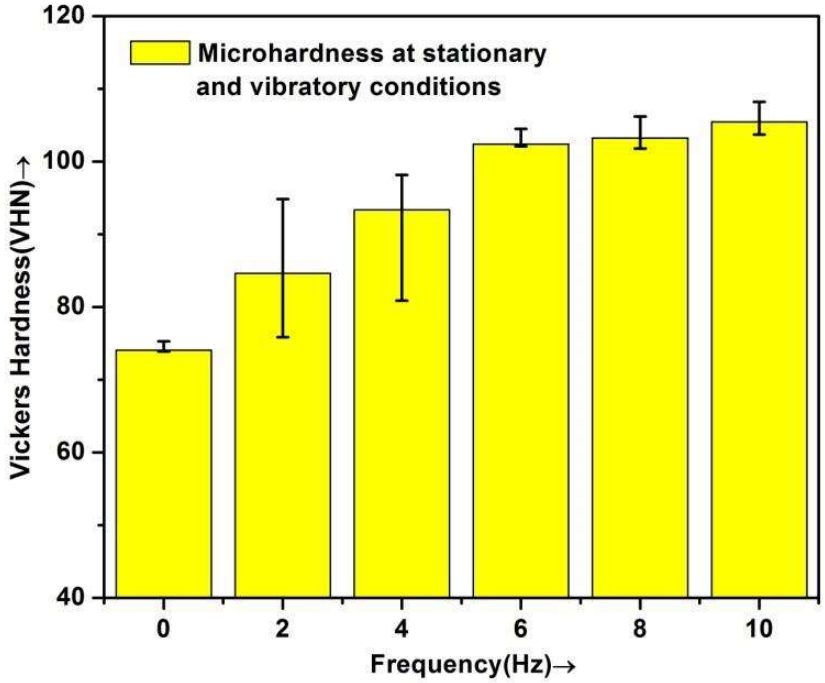

Figure 4.6: Vickers hardness graph of A308 alloy under (a) stationary condition, (b) 2 Hz, (c) 4 Hz, (d) 6 Hz, (e) 8 Hz and (f) 10 Hz frequencies.

Microhardness values were increased due to a much-refined microstructure ascribed to the fast-cooling rate of melt as shown in Figure 4.6. Application of mechanical vibration during melt solidification caused fragmentation into dendritic arms. The non-dendritic and equiaxed microstructure, which resulted in a homogeneous fine-grained structure, was created due to these broken arms acting as new nucleation sites and instigating more nucleation[85]. However, under a low solidification rate, the coarse eutectic silicon and secondary eutectic (Al-Fe-Si) were formed in the matrix, which may weaken the structure of the alloy. But in the present observation, an increase in the frequency up to 10 Hz, the solidification rate increases as shown in Table 4.2, and formations of refined eutectic silicon phases and reduced sized α-Al phase evolved. Further, due to turbulence and convection effect, the intermetallic phases like Al_2Cu and $Fe_{1.7}SiAl_4$, respectively, and

refined eutectic silicon are dispersed uniformly, and improvement was achieved. Inter-metallic compounds possess a high melting point and are brittle also [47, 91].

4.6 Fractography

The tensile fractured (SEM) images of the stationary cast and vibratory cast samples were presented in Figure 4.7(a-f). The tensile fracture behaviour was observed and found that most of the surfaces display transgranular fractures, comprising brittle and cleavage facets, the microstructure improvements and mechanical properties have a favourable response after vibration. Under the brittle fracture mode cleavage facets and brittle facets were visible throughout all the fractographic images, as shown in Figures 4.7(a-f). Fig.4.7 (a) illustrates that the tensile fracture surfaces prepared under stationary conditions reveal a transgranular brittle fracture with brittle facets, grape-like dendrite cells and shrinkage porosities. As demonstrated in Figure 4.7(a), the cracked samples produced under the initial vibratory condition of 2 Hz had brittle facets and microvoids and transgranular type fracture. The fracture surface shows the micro-cracks in the eutectic silicon, as shown in Figure 4.7(c). The rupture occurred along with hard eutectic silicon, and Fe-intermetallic phases show the brittle and cleavage facets along with some ductile tears, as shown in Figure 4.7(d).

The fractured surface morphology also shows the deboning of intermetallic phases (Eutectic Si particles, Al_2Cu, and other impurities like Mn, Fe, Ni) from the Al-matrix, causing initiation of crack propagation. Figure 4.7(c-d) illustrates the intermediate vibration mode at 6 and 8 Hz. The fractured surfaces show the brittle fracture mode with several features like micro-cracks, micro-voids, brittle facets, and ductile tearing, indicating the mixed-mode fracture behaviour. At 10 Hz, the fracture images presented in Figure 4.7(f) showed ductile tearing, and brittle facet structures were observed in

mixed-mode of fracture. The observations and analysis of the SEM fractured images at stationary and vibratory castings; can be seen that at a higher frequency (10 Hz) level, the grain refinements are better due to dendritic fragmentations and nucleation; subsequently, the mechanical properties will increase [92] .

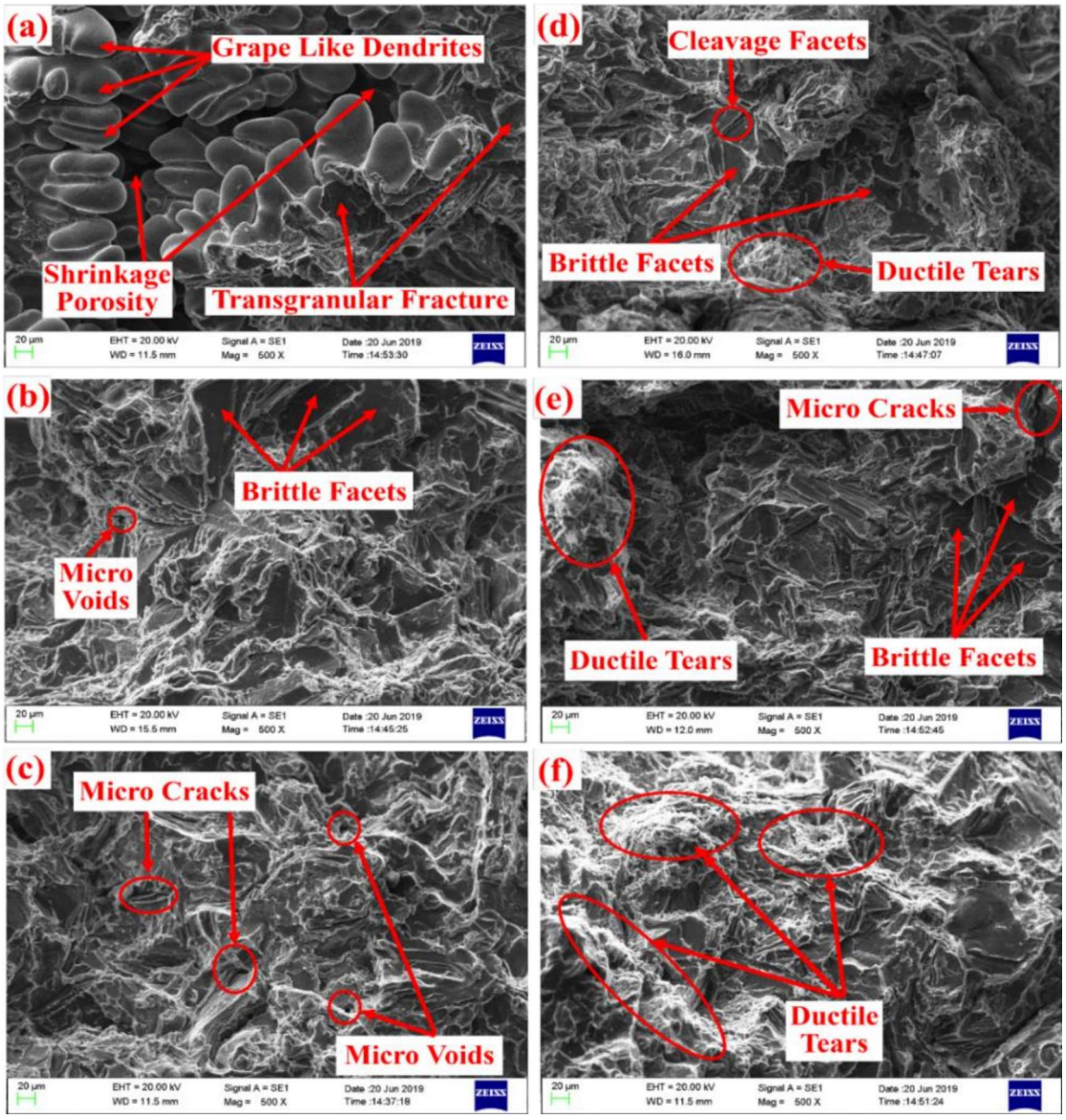

Figure 4.7: Fractography images of tensile test samples (a) stationary condition, (b) 2 Hz, (c) 4 Hz, (d) 6 Hz, (e) 8 Hz and (f) 10 Hz.

4.7 Summary

Using the horizontal mould vibration technique, the combined influence of amplitude and frequency on the physical, metallurgical, and mechanical properties of the A308 alloy was investigated. Cast A-308 alloy characteristics were examined under as-cast and vibratory conditions. The following observations can be summarized as follows:

1. The XRD analysis revealed elements such as Al, Si, Cu, Fe, Mn, and Mg, along with intermetallic compounds such as $Fe_{1.7}SiAl_4$ and Al_2Cu. These elements, were also observed by EDS and spectrometer analysis.
2. At 10 Hz frequency, 21% improvement in cooling rate due to forced convection and 84% reduction in porosity due to better mass feeding and reduced porosities causes the density to increase by 2.5% as compared to conventional casting.
3. The α-Al, SDAS, length, width, and aspect ratio of eutectic Si particles of A-308 alloy at 10 Hz frequency were reduced by 53%, 63%, 71%, 18%, 62% respectively, whereas the shape factor was improved by 39% compared to statically cast alloy.
4. The mechanical properties of A308 alloy obtained through vibratory casting improved steadily with increasing frequency intervals up to a maximum frequency of 10 Hz, with YS, UTS, %EL, and HV reported to be 16%, 25%, 17%, and 42% better than those obtained by statically casting.
5. In the as-cast condition, the fracture surfaces of A308 alloy revealed a distinct brittle fracture mode as a transgranular fracture due to the coarse microstructure. As compared to static casting fracture surfaces, vibratory casting fracture surfaces display mixed-mode fracture behaviour.